A Study of Particle Acceleration in Blazar Jets

Hubing Xiao[1] , Wenxin Yang[2,3,4], Yutao Zhang[2], Shaohua Zhang[1] , Junhui Fan[2,3,4] , Liping Fu[1], and Jianghe Yang[2,5]

[1] Shanghai Key Lab for Astrophysics, Shanghai Normal University, Shanghai 200234, People's Republic of China; hubing.xiao@shnu.edu.cn
[2] Center for Astrophysics, Guangzhou University, Guangzhou 510006, People's Republic of China; fjh@gzhu.edu.cn
[3] Key Laboratory for Astronomical Observation and Technology of Guangzhou, Guangzhou 510006, People's Republic of China
[4] Astronomy Science and Technology Research Laboratory of Department of Education of Guangdong Province, Guangzhou 510006, People's Republic of China
[5] Department of Physics and Electronics Science, Hunan University of Arts and Science, Changde 415000, People's Republic of China
Received 2024 January 10; revised 2024 March 18; accepted 2024 March 26; published 2024 April 29

Abstract

The particle acceleration of blazar jets is crucial to high-energy astrophysics, yet the acceleration mechanism division in blazar subclasses and the underlying nature of these mechanisms remain elusive. In this work, we utilized the synchrotron spectral information (synchrotron peak frequency, $\log \nu_{sy}$, and corresponding curvature, b_{sy}) of 2705 blazars from the literature and studied the subject of particle acceleration in blazar jets by analyzing the correlation between $\log \nu_{sy}$ and $1/b_{sy}$. Our results suggested that the entire sample follows an energy-dependent probability acceleration (EDPA). Specifically, the low inverse Compton peak sources (LCPs) follow the mechanism of fluctuations of fractional gain acceleration (FFGA), while the high inverse Compton peak sources (HCPs) follow an acceleration mechanism of EDPA. Our results indicated that the separation between LCPs and HCPs results from the electron peak Lorentz factor (γ_p), and the differentiation should originate from different acceleration mechanisms. Moreover, our study revealed a transition in the acceleration mechanism from FFGA to EDPA around $\log \nu_{sy} \sim 15$ through a detailed analysis of binned-$\log \nu_{sy}$. The mechanism of FFGA dominates the particle acceleration in LCP jets because of stronger jets and the EDPA dominates the particle energy gain in the HCPs due to a more efficient acceleration process.

Unified Astronomy Thesaurus concepts: Blazars (164); Relativistic jets (1390)

1. Introduction

Referring to the most distinctive and potent active galactic nuclei, blazars manifest exceptional observational properties. Notably, blazars exhibit multifaceted rapid variability across the entire wavelength bands, conspicuous high and variable polarization, powerful γ-ray emissions, apparent superluminal motion, and a confirmed core-dominated emission profile, as substantiated by a plethora of works (Wills et al. 1992; Fan 2002; Villata et al. 2006; Fan et al. 2014, 2021; Gupta et al. 2016; Xiao et al. 2019; Abdollahi et al. 2020; Pei et al. 2020; Xiao et al. 2022b). These distinctive properties are ascribed to the presence of a powerful relativistic jet, which is pointing toward the observer, ensconced within the central supermassive black hole. Blazars are categorized into two distinct subclasses: BL Lacertae objects (BL Lacs) and flat spectrum radio quasars (FSRQs). Their emissions span from the radio to the very high-energy bands, exhibiting a characteristic bimodal structure in the spectral energy distribution (SED).

The broadband SED can be described by the radiation through relativistic particles interacting with magnetic fields, soft photons, or self-interactions and generating secondary particles and cascade process, namely, the leptonic model (Blandford & Koenigl 1979; Sikora et al. 1994; Błażejowski et al. 2000; H.E.S.S. Collaboration et al. 2015; Xue et al. 2019) and the hadronic model (Mücke & Protheroe 2001; Dimitrakoudis et al. 2012; Diltz et al. 2015). A common question in both blazar radiation mechanisms revolves around understanding the particle acceleration mechanism—how do these

relativistic particles grow energy? The observation that the radio-ultraviolet spectrum of blazars can be well-described by a log-parabolic function, as found by Landau et al. (1986), is suggested to be linked to the particle acceleration mechanism, such as first-order Fermi acceleration. Subsequent studies extended this observation to the X-ray spectrum of blazars like Mrk 421 (Massaro et al. 2004a) and Mrk 501, indicating a (quasi-)log-parabolic electron energy distribution (Massaro et al. 2004b). Massaro et al. (2004a) considered a simple statistical mechanism of particle energy gain, which could occur in a shock wave or a strong perturbation moving down a jet. If the probability that a particle undergoes an acceleration step i, in which it has an energy gain independent of energy, then a power-law particle energy spectrum follows, otherwise, an energy-dependent probability acceleration (EDPA) forms a log-parabolic particle energy spectrum. Instead of the acceleration probability being dependent on the particle energy, Tramacere et al. (2011) addressed the mechanism that fluctuations of fractional gain acceleration (FFGA) can form a log-parabolic particle energy spectrum. In the framework of stochastic acceleration, Kardashev (1962) utilized the Fokker–Planck equation in the momentum-diffusion term and suggested that a "quasi-"monoenergetic particle injection can lead to a log-parabolic particle energy spectrum.

The anticorrelation between the synchrotron peak frequency ν_{sy} and the curvature b_{sy} has been identified (Massaro et al. 2006), and exploring the correlation between these two parameters can provide insights into the particle acceleration processes in blazar jets (Tramacere et al. 2007; Paggi et al. 2009). Chen (2014) summarized the correlation between $\log \nu_{sy}$ and $1/b_{sy}$ in different particle acceleration scenarios: (i) $\log \nu_{sy} \approx 2/(5b_{sy}) + C$ for the case of EDPA; (ii) $\log \nu_{sy} \approx 3/(10b_{sy}) + C$ for the case of FFGA; (iii)

$\log \nu_{\mathrm{sy}} \approx 1/(2b_{\mathrm{sy}}) + C$ for the case of quasi-monoenergetic particle injection in the framework of stochastic acceleration. Chen (2014) further studied the correlation between $\log \nu_{\mathrm{sy}}$ and $1/b_{\mathrm{sy}}$ and found a slope of 2.04. Their result suggested that the stochastic acceleration mechanism dominates the particle acceleration in blazar jets. In a study by Tan et al. (2020), a sample of 60 FSRQs yielded $1/b_{\mathrm{sy}} \propto 3.22 \log \nu_{\mathrm{sy}}$, consistent with the statistical acceleration of FFGA. Similarly, Chen et al. (2023a) used a sample of 798 sources (504 FSRQs, 277 BL Lacs, and 17 γNLS1s), and obtained $1/b_{\mathrm{sy}} \propto 2.63 \log \nu_{\mathrm{sy}}$ for all blazars in their sample, $1/b_{\mathrm{sy}} \propto 2.55 \log \nu_{\mathrm{sy}}$ for FSRQs, and $1/b_{\mathrm{sy}} \propto 2.96 \log \nu_{\mathrm{sy}}$ for BL Lacs. Meanwhile, Yang et al. (2022) used a larger sample of 2705 blazars and found $1/b_{\mathrm{sy}} \propto 1.97 \log \nu_{\mathrm{sy}}$ for blazars, $1/b_{\mathrm{sy}} \propto 2.86 \log \nu_{\mathrm{sy}}$ for FSRQs, and $1/b_{\mathrm{sy}} \propto 2.14 \log \nu_{\mathrm{sy}}$ for BL Lacs.

The reason for causing discrepancies among previous results regarding the particle acceleration mechanism of blazars and their subclasses may be twofold. First, the sample size could be insufficient for a comprehensive study of this subject. Second, there might be an evolution of particle acceleration mechanisms among blazars, contributing to the observed variations in the correlation.

In this work, following the previous works and taking advantage of the latest and largest SED fitting sample from Yang et al. (2022), we aim to statistically study the particle acceleration mechanism and further investigate its evolution in blazars. This paper is structured as follows: In Section 2 we present our sample; we present analysis and results in Section 3; the discussions and conclusions will be given in Section 4.

2. Sample

In order to study the particle acceleration mechanism and its possible evolution in blazars, we collected a sample of Fermi blazars with available synchrotron peak frequency ($\log \nu_{\mathrm{sy}}$) and the corresponding curvature (b_{sy}) from Yang et al. (2022). In total, we have 2705 sources, including 759 FSRQs, 1141 BL Lacs, and 808 blazar candidates of uncertain type (BCUs).

3. Results

As mentioned above, the acceleration mechanism can be tested by investigating the slope of the correlation between the peak frequency and the curvature for a sample of blazars. When the ordinary least square (OLS) bisector linear regression is adopted to the present compilation, a correlation between $1/b_{\mathrm{sy}}$ and $\log \nu_{\mathrm{sy}}$,

$$1/b_{\mathrm{sy}} = (2.39 \pm 0.03)\log \nu_{\mathrm{sy}} - (24.51 \pm 0.39),$$

was obtained with a correlation coefficient $r = 0.81$ and chance probability $p \sim 0$ through Pearson analysis for the entire sample as shown in the upper panel of Figure 1. We excluded sources outside the light-blue shadow, which is defined by $[y - 3^{*}\mathrm{std\_dev}, y + 3^{*}\mathrm{std\_dev}]$, and obtained a "clean" sample. Meanwhile, the "clean" sample was divided into low inverse Compton (IC) peak frequency (LCP; $\log \nu_{\mathrm{IC}} < 22.9$) blazars and high IC peak frequency (HCP; $\log \nu_{\mathrm{IC}} \geqslant 22.9$) blazars based on Yang et al. (2023), the correlation between $1/b_{\mathrm{sy}}$ and $\log \nu_{\mathrm{sy}}$ for the LCPs and the HCPs are shown in the lower panel of Figure 1, the regression results

$$1/b_{\mathrm{sy}} = (3.21 \pm 0.08)\log \nu_{\mathrm{sy}} - (35.24 \pm 1.02),$$
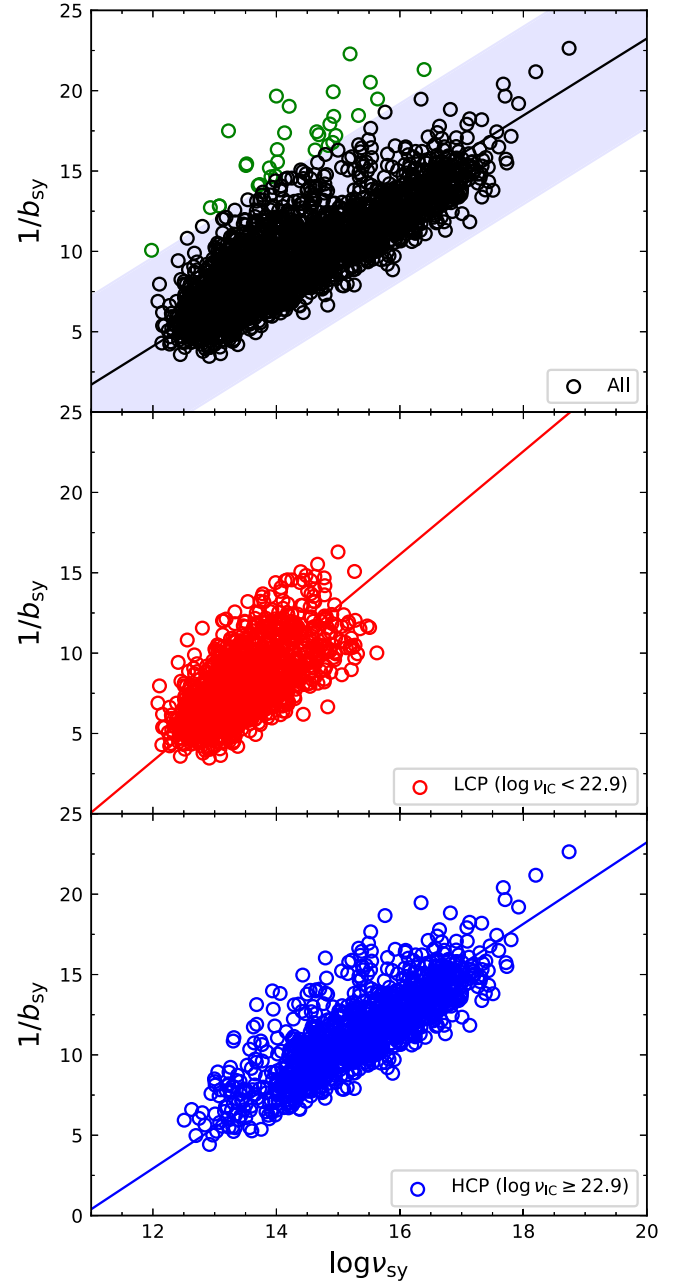
Figure 1. The correlation between $1/b_{\mathrm{sy}}$ and $\log \nu_{\mathrm{sy}}$. The correlation studies are investigated for all sources in our sample (in the upper panel), the light-blue shadow shows a $[y - 3^{*}\mathrm{std\_dev}, y + 3^{*}\mathrm{std\_dev}]$ interval and the green circles outside the shadow are scatters. LCPs without scatters are shown in the middle panel; HCPs without scatters are shown in the bottom panel. The solid lines represent the best regression results.

with $r = 0.65$ and chance probability $p \sim 0$ for the LCPs;

$$1/b_{\mathrm{sy}} = (2.54 \pm 0.04)\log \nu_{\mathrm{sy}} - (27.51 \pm 0.66),$$

with $r = 0.81$ and chance probability $p \sim 0$ for the HCPs.

To investigate the possible evolution of the particle acceleration mechanism in blazars, we assume $1/b_{\mathrm{sy}} = \beta \log \nu_{\mathrm{sy}} + \alpha$. Subsequently, we calculate β for sources falling within each bin ranging from $\log \nu_{\mathrm{sy}}$ to $\log \nu_{\mathrm{sy}} + 3$, $\log \nu_{\mathrm{sy}}$ is increased incrementally by 1 to establish distinct bins for computing β. The corresponding statistical results are shown in Figure 2 and detailed in Table 1.
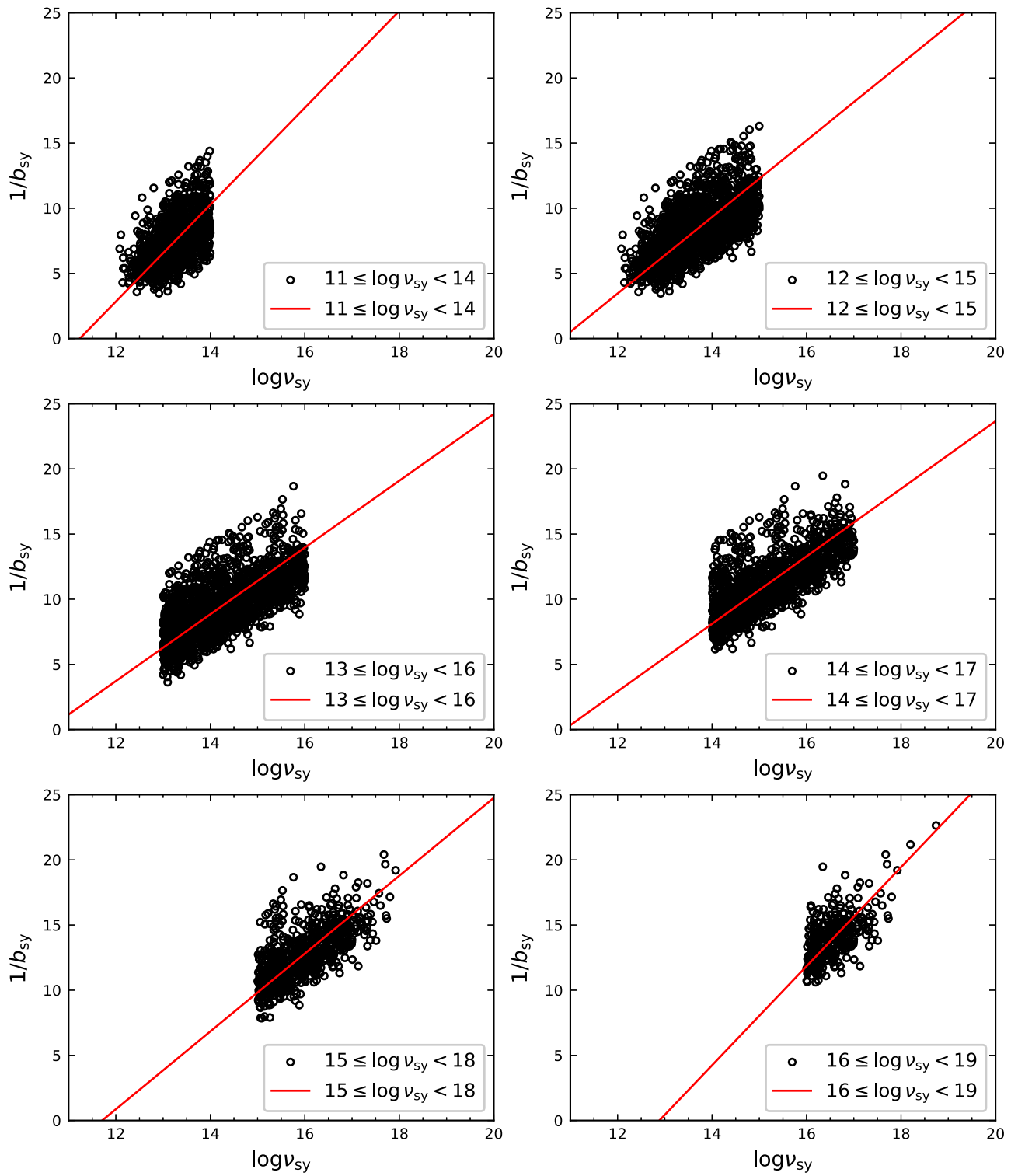
Figure 2. The correlation between $1/b_{\rm sy}$ and $\log \nu_{\rm sy}$. The red solid line represents the best OLS linear regression.

Table 1
The Evolution of β for Sources with Increasing $\log \nu_{\mathrm{syn}}$

Bin ID (1)	Energy Range (2)	N (3)	β (4)	α (5)	r (6)	p (7)
1	$11 \leqslant \log \nu_{\mathrm{sy}} < 14$	1318	3.72 ± 0.12	-41.78 ± 1.64	0.50	9.0×10^{-85}
2	$12 \leqslant \log \nu_{\mathrm{sy}} < 15$	1903	2.94 ± 0.06	-31.79 ± 0.76	0.64	3.2×10^{-224}
3	$13 \leqslant \log \nu_{\mathrm{sy}} < 16$	1970	2.56 ± 0.04	-27.03 ± 0.58	0.70	3.0×10^{-290}
4	$14 \leqslant \log \nu_{\mathrm{sy}} < 17$	1313	2.59 ± 0.05	-28.17 ± 0.70	0.70	1.3×10^{-197}
5	$15 \leqslant \log \nu_{\mathrm{sy}} < 18$	769	2.99 ± 0.08	-34.98 ± 1.25	0.67	6.6×10^{-102}
6	$16 \leqslant \log \nu_{\mathrm{sy}} < 19$	343	3.80 ± 0.19	-48.97 ± 3.08	0.61	6.7×10^{-37}

Note. Column (1) gives the range ID; column (2) gives the range of taking sources; column (3) is the number of the sources in the corresponding range; column (4) gives the β; column (5) gives the α; column (6) gives the Pearson correlation coefficient; column (7) gives the chance probability.

4. Discussion

4.1. The Physical Meaning of the Dividing Boundary with $\log \nu_{\mathrm{IC}}$

In the frame of a leptonic model, the synchrotron peak frequency is written as

$$\nu_{\mathrm{sy}} = 3.7 \times 10^6 \, \gamma_{\mathrm{p}}^2 \, B \, \frac{\delta}{1+z} \, \mathrm{Hz}, \qquad (1)$$

where B is the magnetic field strength in units of Gauss (Tavecchio et al. 1998), γ_{p} is the Lorentz factor of electrons that contribute most to the synchrotron peak, and δ is a Doppler beaming factor. In the Thomson regime, the peak frequency of the IC peak frequency is given by

$$\nu_{\mathrm{SSC}} = \frac{4}{3} \, \gamma_{\mathrm{p}}^2 \, \nu_{\mathrm{sy}}, \qquad (2)$$

in the case of the synchrotron self-Compton (SSC) model; while in the case of the external Compton (EC) process, soft photons are fed externally, and the peak frequency is given by

$$\nu_{\mathrm{EC}} = \frac{4}{3} \, \gamma_{\mathrm{p}}^2 \, \nu_{\mathrm{ext}} \, \frac{\Gamma \delta}{1+z}, \qquad (3)$$

where ν_{ext} is the frequency of external photons, $\nu_{\mathrm{ext}} = 2.46 \times 10^{15}$ Hz for the case of external photons coming from the broad-line region and $\nu_{\mathrm{ext}} = 7.7 \times 10^{13}$ Hz for the case of external photons coming from the dusty torus (Tavecchio & Ghisellini 2008; Ghisellini & Tavecchio 2015), and Γ is a bulk Lorentz factor.

Yang et al. (2023) estimated the IC peak frequency (ν_{IC}) by fitting the IC bump with a parabolic function, studied the distribution of $\log \nu_{\mathrm{IC}}$, and found a bimodal structure via the Bayesian method. They suggested using $\log \nu_{\mathrm{IC}} = 22.9$ to separate blazars into two classes, namely the LCP ($\log \nu_{\mathrm{IC}} < 22.9$) blazars and HCP ($\log \nu_{\mathrm{IC}} \geqslant 22.9$) blazars, while the nature of separating the LCPs and the HCPs remains unclear. The extragalactic background absorption (EBL), in the high- and very high-energy γ-ray bands, could affect the location of the IC peak; the neglection or underestimation of EBL could bias the ν_{IC} and consequently affect the separation value.

The LCPs are distributed tighter than the HCPs in the space of $\log \nu_{\mathrm{sy}}$, and the HCPs should have an averagely larger $\log \nu_{\mathrm{sy}}$ than the LCPs, as seen in the middle and bottom panels of Figure 1. Equation (1) indicates that the synchrotron peak frequency primarily depends on δ, B, and γ_{p}, and a

comprehensively joint effort of these three parameters results in the divergence in $\log \nu_{\mathrm{sy}}$. The Doppler beaming factor, δ, has been consistently estimated in various studies, yielding values around ~ 10 s for the majority of blazars (e.g., Liodakis et al. 2018; Zhang et al. 2020; Pei et al. 2022; Xiao et al. 2022a). Consequently, a dispersion in δ is not expected to be the main reason for demonstrating the difference in $\log \nu_{\mathrm{sy}}$. In our recent work, Fan et al. (2023) estimated B and γ_{p} for blazars with certain classes and they provided lower and upper limits of B and γ_{p} for those BCUs by treating these sources as FSRQs and BL Lacs, respectively. We obtained the values of B and γ_{p} for BCUs using the predicted class assigned by the fractal dimension–inverse discrete wavelet transform method introduced in Cao et al. (2024). Figure 3 illustrates the distribution of B and γ_{p} for the HCPs and the LCPs. The analysis reveals that the LCPs have $\log B = -0.39 \pm 1.50$, while the HCPs have $\log B = -0.29 \pm 1.39$. A Student t-test yields $p = 0.08$, indicating that the hypothesis of these two samples having identical average values cannot be rejected. Therefore, B is also not the main reason separating the LCPs and the HCPs in $\log \nu_{\mathrm{sy}}$. Then, the focus shifts to γ_{p}, and, as depicted in the lower panel of Figure 3, it is evident the HCPs and parts of the LCPs have an averagely larger $\log \gamma_{\mathrm{p}}$ than the majority of the LCPs.

Based on Equations (2) and (3), this differentiation in $\log \gamma_{\mathrm{p}}$ directly translates to the divergence in IC peak frequency $\log \nu_{\mathrm{IC}}$ between HCPs and LCPs. In the case of the SSC process, it is evident that the value of ν_{SSC} mainly depends on γ_{p} because, as we have mentioned above, ν_{sy} is mainly affected by γ_{p}. In the case of the EC process, the cooling process from seed photons, namely ν_{ext}, also plays an important role in determining ν_{EC}. The cooling effect has been counted in the estimation of B and γ_{p} in Fan et al. (2023), where we obtained the values of B and γ_{p} for the discussions presented in this work. To sum up, the separation in $\log \nu_{\mathrm{IC}}$ between LCP and HCP mainly stems from the dispersion in γ_{p}.

4.2. Particle Acceleration in Blazar Jets

Based on the sample, we studied the correlation between $1/b_{\mathrm{sy}}$ and $\log \nu_{\mathrm{sy}}$. Our findings reveal a relationship characterized by $1/b_{\mathrm{sy}} \propto 2.39 \log \nu_{\mathrm{sy}}$, indicative of particle acceleration in blazar jets occurring with EDPA. Furthermore, this correlation implies a trend toward smaller curvatures as the synchrotron peak frequency increases. This is attributed to the shorter cooling timescale compared to the timescales for acceleration (Tramacere et al. 2009).
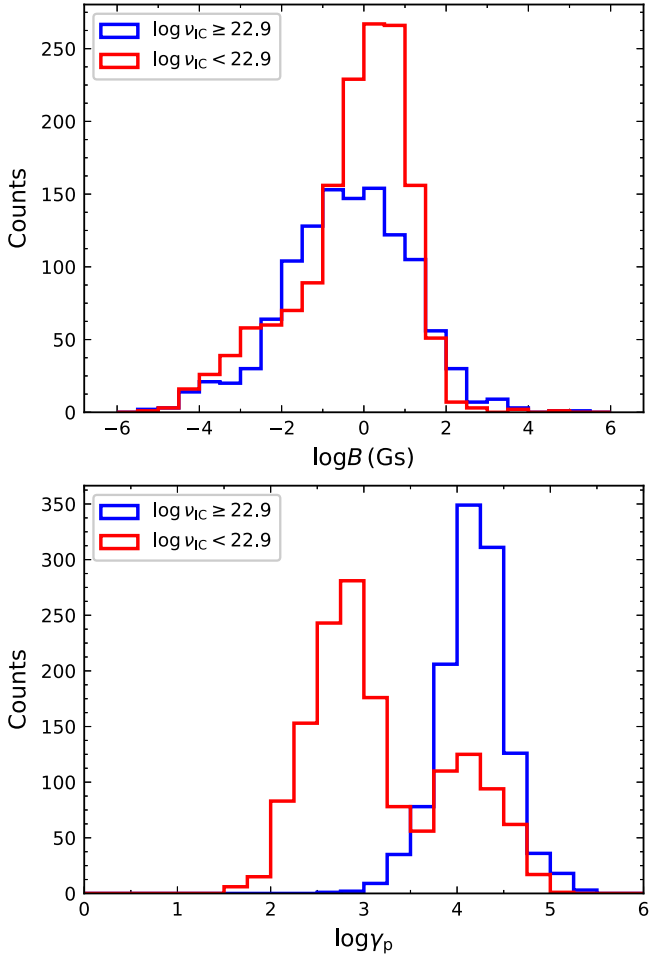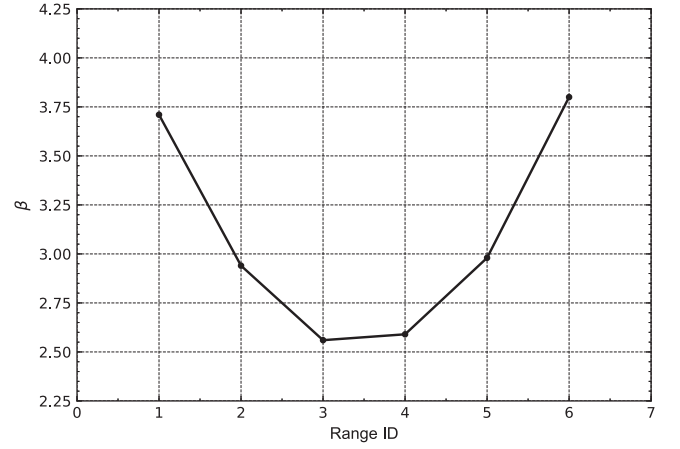
Figure 3. The correlation between $1/b_{sy}$ and $\log \nu_{sy}$. The red histogram stands for the sources with $\log \nu_{IC} < 22.9$, and the blue histogram stands for the sources with $\log \nu_{IC} \geqslant 22.9$.

Figure 4. The slope of correlation $1/b_{sy}$ against $\log \nu_{sy}$ in the range of $[\log \nu_{sy}, \log \nu_{sy} + 3)$.

There are 31 scatters, with relatively large $1/b_{sy}$ in the entire sample, which are marked in green in the upper-left region of the upper panel of Figure 1. These scatters are caused by the lack of X-ray data, resulting in a consequent insufficient constraint on the fitting of the synchrotron bump and a small value of curvature b_{sy}. In the middle and bottom panels of Figure 1, the sources are divided with the boundary of $\log \nu_{IC} = 22.9$. The value of the boundary is intricately linked to the B, δ, and γ_p and is mainly determined by γ_p; we found that the particles in LCP jets are accelerated with FFGA and in HCP jets are accelerated in the form of EDPA. Moreover, the acceleration mechanism of EDPA is more efficient than FFGA, because the HCPs have an averagely larger $\log \gamma_p$ than the LCPs, as shown in the middle and bottom panels of Figure 1.

If the separation between LCPs and HCPs is caused by the difference in the electron Lorentz factor, resulting from distinct particle acceleration mechanisms. The transition, which should not be accomplished suddenly but gradually, from one mechanism to another is expected to leave tracks.

To explore the possible evolution or transition between these acceleration mechanisms, we divided the sample into six bins for $\log \nu_{sy}$ with IDs ranging from 1 to 6. We then examined the slope (β) for each bin, with the results presented in Table 1 and illustrated in Figure 2. The change of β is illustrated in Figure 4; it is clear that β decreases from 3.71 to 2.56 and subsequently increases to 3.80. The values of 3.71 and 3.80,

corresponding to "Bin 1" and "Bin 6," should be assessed very carefully because these two bins contain borders and the quantity of the sources near the bin border may significantly influence the slope. In general, the FFGA mechanism seems to dominate the sources with relatively small $\log \nu_{sy}$, then the EDPA mechanism starts to dominate when the $\log \nu_{sy}$ gets larger.

The first acceleration mechanism transitions from FFGA to EDPA in Figure 4, namely the slope change from "Bin 2" to "Bin 3" or "Bin 4," and the transition likely occurs at $\log \nu_{sy} \sim 15$. Interestingly, most of the LCPs occupy the region $\log \nu_{sy} \lesssim 15$ and the HCPs occupy the region $\log \nu_{sy} \gtrsim 15$. Thus, the first acceleration mechanism transition in Figure 4 is consistent with the acceleration mechanism transition from the LCPs to the HCPs, we suggest the first transition in Figure 4 is interpreted as the separation of $\log \gamma_p$.

However, the second transition from EDPA to FFGA in Figure 4, namely the slope change from "Bin 3" or "Bin 4" to "Bin 5" or "Bin 6," may be caused by those sources near the bin border and should be carefully taken as a real transition, as we can see in the bottom-left panel of Figure 2.

4.3. The Acceleration Mechanism

According to our results, the statistical acceleration mechanism dominates the energy gain of particles in the blazar jets, and the mechanism transition is derived. In the framework of statistical acceleration, the EDPA mechanism was discussed in Massaro et al. (2004a). In this mechanism, the accelerated particle's energy is expressed as $\gamma_i = \varepsilon \gamma_{i-1}$, in which the energy gain ε of acceleration step i is independent of energy and assumed to be constant. However, the probability of the particle undergoing the acceleration step i is dependent on the particle energy as $p_i = g/\gamma_i^q$, where g and q are positive constants. Thus, a particle with a initial Lorentz factor γ_0 undergoing n step of acceleration has a probability of

$$\Pi_{i=0}^n p_i = g^n / \Pi_{i=0}^n \gamma_i^q = g^n / [\gamma_0^{nq} \varepsilon^{\frac{n(n-1)}{2} q}]. \quad (4)$$

This leads to the final accelerated energy

$$\gamma_n = \varepsilon^n \gamma_0. \quad (5)$$

An alternative mechanism known as FFGA was introduced by Tramacere et al. (2011). In the FFGA model, the energy gain is expressed as $\gamma_i = \varepsilon_i \gamma_{i-1}$, where $\varepsilon_i = \bar{\varepsilon} + \chi_i$. Here, $\bar{\varepsilon}$

represents the systematic energy gain, and χ_i is a random variable with a probability density function with a zero mean value ($\langle\chi\rangle = 0$) and a variance of δ_χ. For a particle with an initial Lorentz factor γ_0 undergoing n steps of acceleration in the FFGA model, the expected final Lorentz factor is given by

$$\gamma_n = \gamma_0 \Pi_{i=0}^n \varepsilon_i = \gamma_0 \Pi_{i=0}^n (\bar{\varepsilon} + \chi_i) = \gamma_0 \bar{\varepsilon}^n \Pi_{i=0}^n (1 + \chi_i/\bar{\varepsilon}). \tag{6}$$

Taking into account that both EDPA and FFGA mechanisms are simultaneously at play in blazar jets, the dominance of one over the other depends on the specific blazar subclass. For LCPs, FFGA appears to be the dominant mechanism, while EDPA is more prominent in HCPs. In both acceleration mechanisms, the accelerated particle's energy is influenced by the number of acceleration steps (n). This parameter serves as a crucial variable determining the final Lorentz factor (γ_n) in both scenarios, as described by Equations (5) and (6).

For a given synchrotron intensity with corresponding electron Lorentz factor γ_p, the formation of relativistic particles through EDPA involves two possible approaches: (1) according to Equation (4), a substantial number of particle supplements is provided due to the decreasing acceleration probability with each acceleration step i. In this scenario, one should anticipate a greater supply of material to provide more seed electrons, and thus those sources with a higher accretion ratio (e.g., FSRQ; Ghisellini et al. 2011; Sbarrato et al. 2012; Pei et al. 2022; Xiao et al. 2022a) should have this privilege; (2) alternatively, with a relatively large energy gain ε in each step of acceleration, the acceleration process becomes more efficient, and particles can attain γ_p in fewer steps before the acceleration probability diminishes. We found that the particle acceleration in HCP jets is dominated by EDPA, while the HCPs primarily consist of BL Lacs, which are believed to have a smaller accretion ratio. Thus, the acceleration may be more efficient in the jets of HCPs and particles gain energy significantly in each acceleration process.

Similarly, for a given synchrotron intensity with corresponding electron Lorentz factor γ_p. According to Equation (6), the particles can be accelerated to γ_p efficiently when the χ_i is significantly positive more often than negative in the case of FFGA. This condition indicates a relatively strong acceleration process. In this work, we noticed that the particle acceleration in LCP jets is dominated by FFGA, and the 1500 LCPs in this work (consisting of 705 FSRQs, 538 BCUs, and 257 BLLs) are mainly constructed by FSRQs. This preference for a relatively strong acceleration process aligns with the understanding that FSRQs generally exhibit higher jet power compared to BL Lacs (Chen et al. 2023b).

5. Conclusion

In this work, for the purpose of studying the particle acceleration mechanism in blazar jets, we conducted an analysis of the correlation between $1/b_{sy}$ and $\log\nu_{sy}$ for the entire sample and its subgroups (LCP and HCP). Our findings can be summarized as follows: (1) a slope of 2.39 indicates an EDPA for the entire sample, a slope of 3.21 indicates an FFGA for the LCP, and a slope of 2.54 indicates an EDPA for the HCP; (2) the separation between LCPs and HCPs is attributed to the distinct γ_p values between the two subclasses; (3) further exploration of the particle acceleration mechanism involved an investigation of the slope changes in different $\log\nu_{sy}$ bins. This analysis revealed an acceleration mechanism transition from FFGA to EDPA around $\log\nu_{sy} \sim 15$; (4) a comparison between EDPA and FFGA suggested that EDPA is more efficient in the HCPs, where particles experience significant energy gain in each acceleration process. Conversely, in LCPs, a stronger acceleration process operates through FFGA due to the presence of more powerful jets.

ORCID iDs

Hubing Xiao ⓘ https://orcid.org/0000-0001-8244-1229
Shaohua Zhang ⓘ https://orcid.org/0000-0001-8485-2814
Junhui Fan ⓘ https://orcid.org/0000-0002-5929-0968
Jianghe Yang ⓘ https://orcid.org/0000-0002-4469-9672

References

Abdollahi, S., Acero, F., Ackermann, M., et al. 2020, ApJS, 247, 33
Blandford, R. D., & Koenigl, A. 1979, ApL, 20, 15
Błażejowski, M., Sikora, M., Moderski, R., & Madejski, G. M. 2000, ApJ, 545, 107
Cao, H., Xiao, H., Luo, Z., Zeng, X., & Fan, J. 2024, ApJ, 961, 91
Chen, L. 2014, ApJ, 788, 179
Chen, Y., Gu, Q., Fan, J., et al. 2023a, ApJ, 944, 157
Chen, Y., Gu, Q., Fan, J., et al. 2023b, ApJS, 268, 6
Diltz, C., Böttcher, M., & Fossati, G. 2015, ApJ, 802, 133
Dimitrakoudis, S., Mastichiadis, A., Protheroe, R. J., & Reimer, A. 2012, A&A, 546, A120
Fan, J., Xiao, H., Yang, W., et al. 2023, ApJS, 268, 23
Fan, J.-H. 2002, PASJ, 54, L55
Fan, J.-H., Bastieri, D., Yang, J.-H., et al. 2014, RAA, 14, 1135
Fan, J. H., Kurtanidze, S. O., Liu, Y., et al. 2021, ApJS, 253, 10
Ghisellini, G., & Tavecchio, F. 2015, MNRAS, 448, 1060
Ghisellini, G., Tavecchio, F., Foschini, L., & Ghirlanda, G. 2011, MNRAS, 414, 2674
Gupta, A. C., Agarwal, A., Bhagwan, J., et al. 2016, MNRAS, 458, 1127
H. E. S. S. Collaboration, Abramowski, A., Aharonian, F., et al. 2015, A&A, 573, A31
Kardashev, N. S. 1962, SvA, 6, 317
Landau, R., Golisch, B., Jones, T. J., et al. 1986, ApJ, 308, 78
Liodakis, I., Hovatta, T., Huppenkothen, D., et al. 2018, ApJ, 866, 137

Massaro, E., Perri, M., Giommi, P., & Nesci, R. 2004a, A&A, 413, 489
Massaro, E., Perri, M., Giommi, P., Nesci, R., & Verrecchia, F. 2004b, A&A, 422, 103
Massaro, E., Tramacere, A., Perri, M., Giommi, P., & Tosti, G. 2006, A&A, 448, 861
Mücke, A., & Protheroe, R. J. 2001, APh, 15, 121
Paggi, A., Cavaliere, A., Vittorini, V., & Tavani, M. 2009, A&A, 508, L31
Pei, Z., Fan, J., Yang, J., Huang, D., & Li, Z. 2022, ApJ, 925, 97
Pei, Z.-Y., Fan, J.-H., Bastieri, D., et al. 2020, RAA, 20, 025
Sbarrato, T., Ghisellini, G., Maraschi, L., & Colpi, M. 2012, MNRAS, 421, 1764
Sikora, M., Begelman, M. C., & Rees, M. J. 1994, ApJ, 421, 153
Tan, C., Xue, R., Du, L.-M., et al. 2020, ApJS, 248, 27
Tavecchio, F., & Ghisellini, G. 2008, MNRAS, 386, 945
Tavecchio, F., Maraschi, L., & Ghisellini, G. 1998, ApJ, 509, 608

Tramacere, A., Giommi, P., Perri, M., Verrecchia, F., & Tosti, G. 2009, A&A, 501, 879
Tramacere, A., Massaro, E., & Taylor, A. M. 2011, ApJ, 739, 66
Tramacere, A., Massaro, F., & Cavaliere, A. 2007, A&A, 466, 521
Villata, M., Raiteri, C. M., Balonek, T. J., et al. 2006, A&A, 453, 817
Wills, B. J., Wills, D., Breger, M., Antonucci, R. R. J., & Barvainis, R. 1992, ApJ, 398, 454
Xiao, H., Fan, J., Yang, J., et al. 2019, SCPMA, 62, 129811
Xiao, H., Ouyang, Z., Zhang, L., et al. 2022a, ApJ, 925, 40
Xiao, H. B., Zhu, J. T., Fan, J. H., et al. 2022b, MNRAS, 517, 4202
Xue, R., Liu, R.-Y., Wang, X.-Y., Yan, H., & Böttcher, M. 2019, ApJ, 871, 81
Yang, J., Fan, J., Liu, Y., et al. 2023, SCPMA, 66, 249511
Yang, J. H., Fan, J. H., Liu, Y., et al. 2022, ApJS, 262, 18
Zhang, L., Chen, S., Xiao, H., Cai, J., & Fan, J. 2020, ApJ, 897, 10